1 *Article*

# 2 Mapping of Cold-Water Coral Carbonate
# 3 Mounds Based on Geomorphometric Features:
# 4 An Object-Based Approach

5 **Markus Diesing [1],\* and Terje Thorsnes [2]**

6 [1] Geological Survey of Norway, Postal Box 6315 Torgarden, NO-7491 Trondheim, Norway;
7 markus.diesing@ngu.no
8 [2] Geological Survey of Norway, Postal Box 6315 Torgarden, NO-7491 Trondheim, Norway;
9 terje.thorsnes@ngu.no
10 \* Correspondence: markus.diesing@ngu.no; Tel.: +47-7390-4309

11 **Abstract:** Cold-water coral reefs are rich, yet fragile ecosystems found in colder oceanic waters.
12 Knowledge of their spatial distribution on continental shelves, slopes, seamounts and ridge
13 systems is vital for marine spatial planning and conservation. Cold-water corals frequently form
14 conspicuous carbonate mounds of varying sizes, which are identifiable from multibeam
15 echosounder bathymetry and derived geomorphometric attributes. However, the often large
16 number of mounds makes manual interpretation and mapping a tedious process. We present a
17 methodology that combines image segmentation and random forest spatial prediction with the aim
18 to derive maps of carbonate mounds and an associated measure of confidence. We demonstrate our
19 method based on multibeam echosounder data from Iverryggen on the mid-Norwegian shelf. We
20 identified the image-object mean planar curvature as the most important predictor. The presence
21 and absence of carbonate mounds is mapped with high accuracy (overall accuracy = 84.4%,
22 sensitivity = 0.827 and specificity = 0.866). Spatially-explicit confidence in the predictions is derived
23 from the predicted probability and whether the predictions are within or outside the modelled
24 range of values and is generally high. We plan to apply the showcased method to other areas of the
25 Norwegian continental shelf and slope where MBES data have been collected with the aim to
26 provide crucial information for marine spatial planning.

27 **Keywords:** cold-water coral; carbonate mound; habitat mapping; spatial prediction; image
28 segmentation; GEOBIA; random forest; accuracy, confidence

29

## 30 1. Introduction

31 Cold-water coral (CWC) reefs are complex three-dimensional habitats that provide niches for
32 many species and hence are notable for their high biodiversity [1]. Such reefs might also function as
33 nurseries for fish larvae [2] and fish habitat [3], although such claims are contested [4]. Moreover,
34 CWC are of importance as archives of palaeo-environmental changes due to their longevity,
35 cosmopolitan distribution and banded skeletal structure [1].
36 At the same time, human activities threaten these ecosystems in at least three ways [1]: (i)
37 physical damage through demersal fishing [5–8], (ii) potential impacts from hydrocarbon drilling
38 [9,10] and (iii) likely effects of ocean acidification on calcifying reef fauna [11–14]. Therefore,
39 knowledge on the spatial distribution of CWC reefs is vital for effective marine spatial planning and
40 conservation. Deriving the necessary spatial information is typically attempted by spatial
41 distribution modelling for selected framework-forming CWC species [15,16]. However, data on
42 CWC species' presence and absence are often sparse and important predictor variables frequently
43 only exist at a coarse spatial resolution. Consequently, the resulting maps of CWC species
44 distributions are frequently too coarse for many management applications.

45      The geological products of CWC reefs are 'cold-water coral carbonate mounds', positive
46  topographic features that owe their origin, partially or entirely, to the framework-building capacity
47  of CWCs [17]. In the following, we will refer to these structures as carbonate mounds. Such
48  carbonate mounds are identifiable from multibeam echosounder (MBES) data; however, the large
49  number of carbonate mounds that can be seen in MBES data makes manual interpretation and
50  mapping a tedious process.
51      In Norway, 'bioclastic sediments' associated with carbonate mounds have been mapped as part
52  of the MAREANO (Marine AREA database for NOrwegian coast and sea areas) seabed mapping
53  programme. Such maps give a good approximation of the occurrence of carbonate mounds [18].
54  However, for many applications including marine spatial planning and conservation, these products
55  are too generalised as they do not pinpoint individual mounds, nor do they convey the confidence in
56  the map products in a spatially explicit manner.
57      The objectives of this research are therefore to develop a quick, repeatable and validated
58  methodology that allows mapping of carbonate mounds with high spatial detail and that expresses
59  the confidence in the mapped outputs in a spatially explicit way.

60  **2. Materials and Methods**

61  2.1. Site

62      Iverryggen is situated on the mid-Norwegian shelf approximately 75 km west of the
63  Norwegian coast. It is a nearly 20 km long N-S trending ridge (Figure 1), 7 km wide and up to 120 m
64  high [19]. The Iverryggen ridge is interpreted as the product of glacitectonic processes, where
65  compressive subglacial stresses from a westward ice-sheet during the Late Weichselian glaciation
66  caused thrusting and build-up of the ridge. The stresses were induced by basal freezing close to a
67  thin ice-sheet margin. The seabed sediments on the ridge are dominated by gravelly deposits on the
68  highest, central parts of the ridge, with sand and gravelly sand in the fringe areas. Sandy mud and
69  gravelly sandy mud dominate around the ridge [20]. CWC reefs on Iverryggen have been known to
70  fishermen since bottom-trawling started in the area in the 1990s. Following scientific investigations
71  in the late 1990s that indicated extensive trawl damage to the reefs, the area was closed to bottom
72  trawling in 2000 [21].

73  *2.2. Data*

74      Multibeam echosounder (MBES) data were collected and processed by the Norwegian Mapping
75      Authority, Division Hydrographic Service, in April 2012 with a Kongsberg EM710 system onboard
76      the Norwegian survey vessel Hydrograf. The surveyed area has a size of 918 km$^2$. The raw MBES
77      data were processed with software Neptune and a digital elevation model (DEM) with a grid cell size
78      of 5 m produced. Bathymetric derivatives were calculated from the 3x3 Lee-filtered DEM as 32-bit
79      floating point raster files (

80

81      Table 1). Additionally, the bathymetric position index with a radius of 3 pixels (bpi3) was
82  transformed to an 8-bit raster image used for image segmentation (see below). All layers were
83  projected to UTM Zone 33 North.

84
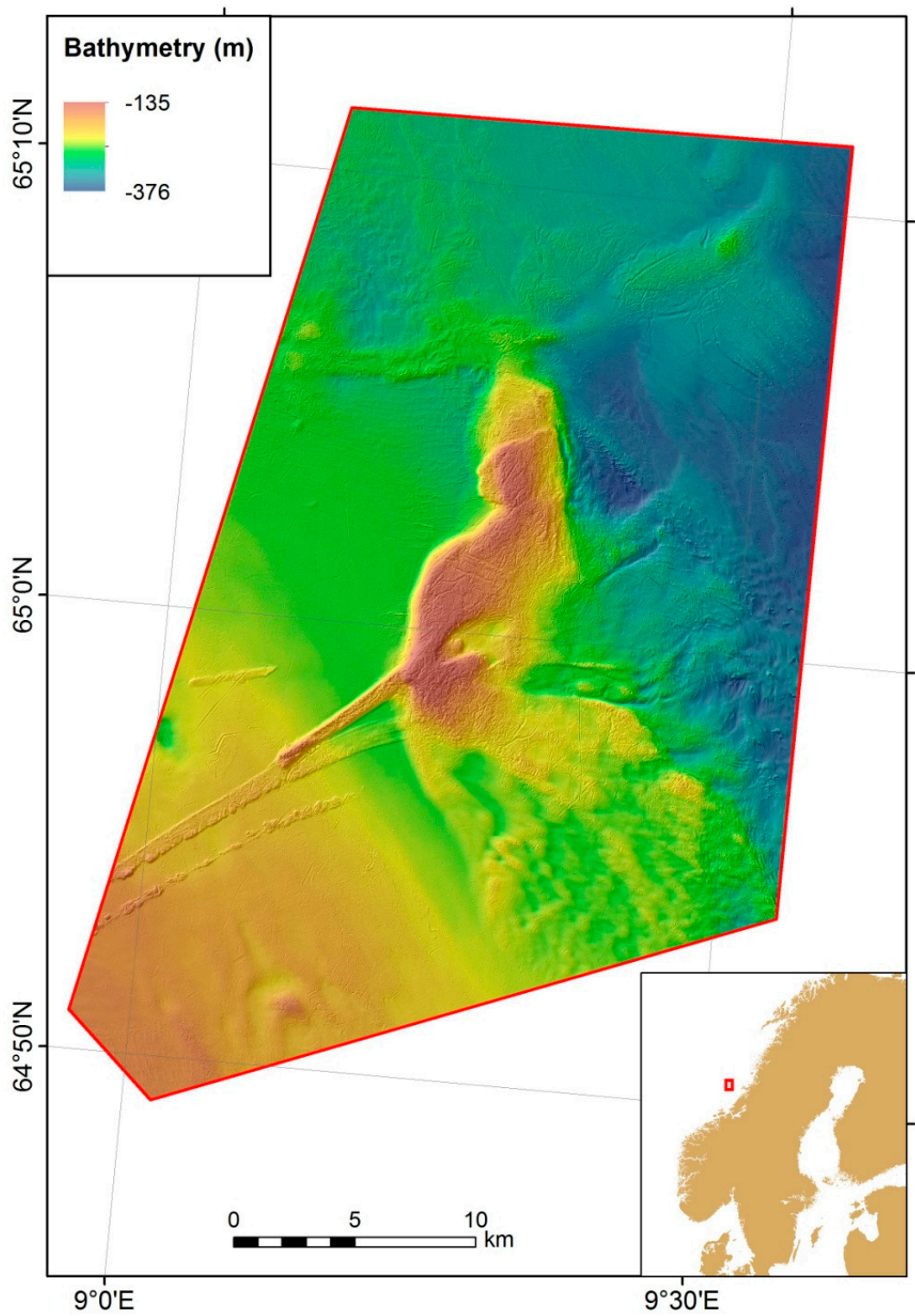
85      Figure 1. Map showing bathymetry in the study site Iverryggen. Inset map shows the location of the
86      study site off the coast of Norway.

87

88

89        Table 1. Bathymetric derivatives utilised in this study.

| Derivative | Description | Abb. | Unit | Reference |
|---|---|---|---|---|
| **Slope** | The maximum slope gradient | slope | ° | [22] |
| **Roughness** | The difference between minimum and maximum of a cell and its eight neighbours. | rgh | m | [22] |
| **Vector ruggedness measure (VRM)** | The variation in three-dimensional orientation of grid cells within a neighbourhood. A radius of 3 pixels was used. | vrm3 | - | [23] |
| **Curvature** | Rate of change of slope. Profile (PR) curvature is measured parallel to maximum slope; plan (PL) curvature is measured perpendicular to slope. | curv curvPL curvPR | - | [22] |
| **Bathymetric position index (BPI)** | Vertical position of a cell relative to its neighbourhood. Radii of 3, 5, 10 and 25 pixels were used. | bpi3 bpi5 bpi10 bpi25 | m | [24] |
| **Zero-mean bathymetry** | A moving mean filter with a rectangular neighbourhood of 25 m by 25 m was applied to the bathymetry layer. The resulting smoothed bathymetry was subtracted from the bathymetry layer. | 0mean | m | [25] |

90

91    A pre-existing shapefile showing bioclastic sediments [18] was used as a spatial constraint. This
92    was extracted from [20]. The layer was derived by visual analysis of MBES data and digitisation and
93    is depicting areas where bioclastic sediments, including those associated with carbonate mounds,
94    are likely to exist. The following analysis was restricted to areas highlighted as bioclastic sediments
95    and a 25-m buffer around these.

96    The general research strategy consisted of three major elements and is outlined in Figure 2:
97    geographic object-based image analysis (GEOBIA) [26,27], visual classification of sample objects and
98    modelling the spatial distribution of carbonate mounds. Initially, image segmentation was carried
99    out to derive image objects (polygons) from suitable raster derivative layers. The aim was to form
100   objects that were either complete mounds (especially smaller ones) or parts of these (e.g. top, slope,
101   foot). In a subsequent step, candidate mounds were defined by applying a simple rule-based
102   classification. These candidate mounds would ideally contain all true mounds, but unavoidably also
103   a certain number of features that have similar characteristics, but are not carbonate mounds. A wide
104   range of object features was extracted for these candidate mounds and used for further analysis.

105   A randomly selected subset of the candidate mounds was visually inspected and classified into
106   objects that either belonged to a carbonate mound or not. This dataset was subsequently split into
107   objects used for feature selection and model fitting and those used to assess the performance and
108   accuracy of the model. Finally, the model was applied to all image objects and mapping confidence
109   was assessed.

110
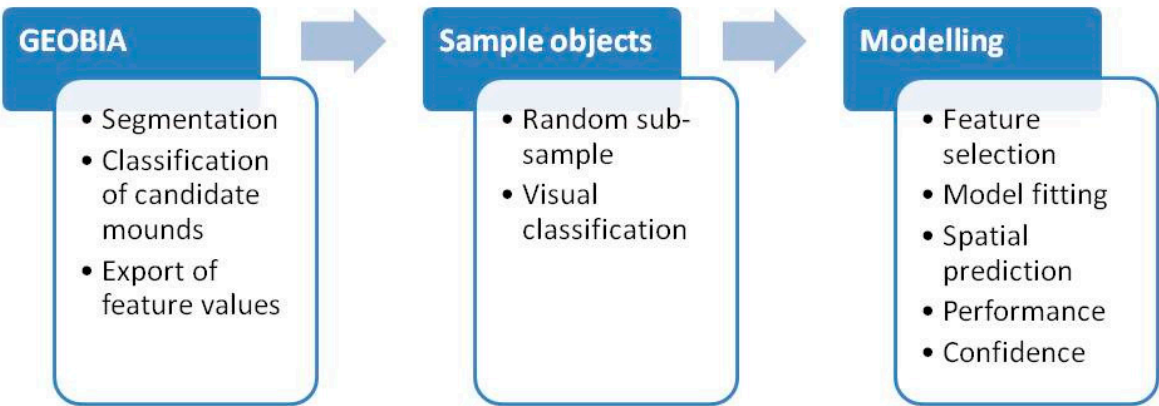
111      Figure 2. General work flow

112    *2.3. Image segmentation*

113      Image segmentation is a vital step in GEOBIA, which is a two-step approach consisting of
114    segmentation and classification. Segmentation is the process of complete partitioning of an image
115    into non-overlapping polygons in image space [28] on the basis of homogeneity [27]. The aim of the
116    segmentation is to divide the image into meaningful polygons of variable sizes, based on their
117    spectral and spatial characteristics. The resulting image objects can be characterised by various
118    features such as layer values (mean, standard deviation etc.), geometry (extent, shape etc.), image
119    texture and many others. Classification is then based on user-specified combinations of these image
120    object features or by applying statistical methods of spatial prediction.

121      Image segmentation was carried out in eCognition 9.2.0 on the BPI3 8-bit layer and the buffered
122    bioclastic sediments shapefile. A multi-resolution segmentation with a scale factor of 10, shape of 0.1
123    and compactness of 0.5 was applied. The selection of the segmentation parameters was made after
124    trialling different combinations and assessing the results visually.

125    *2.4. Classification of candidate mounds*

126      Candidate mounds were classified with the zero-mean bathymetry (

127

128      Table 1) ≥ 0.05 m within buffered areas of bioclastic sediments.

129    *2.5. Export of feature values*

130      Image objects classified as candidate mounds were exported as a shapefile together with 24
131    image-object features (Table 2). These included object mean values of derivatives, maximum pixel
132    values of selected derivatives and geometry features (extent and shape features).

133      Table 2. Image-object features extracted for further analysis. Abbreviations of extent and shape
134      features given in brackets.

| Feature type | Features |
|---|---|
| Object mean value (Mean_...) | slope, rgh, vrm3, curv, curvPL, curvPR, bpi3, bpi5, bpi10, bpi25, 0mean |
| Maximum pixel value (Max_...) | slope, rgh, vrm3, curvPL, bpi3, 0mean |
| Extent | Area (Area_pxl), border length (Border_len), length-width ratio (LengthWidt) |

| **Shape** | Asymmetry, compactness (Compactnes), elliptic fit (Elliptic_f), main direction (Main_direc) |
|---|---|

135   *2.6. Defining sample objects*

136   One thousand image objects were randomly selected using the NOAA Sampling Design Tool
137   (https://www.arcgis.com/home/item.html?id=ecbe1fc44f35465f9dea42ef9b63e785) in ArcGIS 10.4.1.
138   Based on shaded relief and bpi3 maps, image objects were manually classified as belonging to a
139   carbonate mound or otherwise. In total 573 image objects indicated the presence of carbonate
140   mounds and 427 image objects the absence of mounds. The selected sample objects were split into
141   training and test data with a ratio of 2:1 using a stratified random approach to ensure the same class
142   frequencies in both training and test data (Table 3). Subsequent feature selection and model fitting
143   was conducted with the training data, while the test set was used to estimate model performance.

144   Table 3. Number of sample objects in training and test set.

|  | Training | Test | Sum |
|---|---|---|---|
| **Presence (1)** | 382 | 191 | 573 |
| **Absence (0)** | 285 | 142 | 427 |
| **Sum** | 667 | 333 | 1000 |

145   *2.7. Feature selection*

146   The feature selection approach consisted of two steps: Initially, all relevant features were
147   identified with the Boruta algorithm. Subsequently, the set of predictors was reduced to
148   uncorrelated features.
149   The Boruta variable selection wrapper algorithm [29] was employed for the identification of all
150   relevant predictor features. Wrapper algorithms identify relevant features by performing multiple
151   runs of predictive models, testing the performance of different subsets [30]. The Boruta algorithm
152   creates copies of all features and randomises them. These so-called shadow features are added to the
153   predictor feature data set and the Random Forest algorithm (see below) is run to compute feature
154   importance scores for predictor and shadow features. The maximum importance score among the
155   shadow features (MZSA) is determined. For every predictor feature, a two-sided test of equality is
156   performed with the MZSA. Predictor features that have a feature importance score significantly
157   higher than the MZSA are deemed important. Likewise, predictor features that have a variable
158   importance score significantly lower than the MZSA are deemed unimportant. Tentative features
159   have a variable importance score that is not significantly different from the MZSA. The Boruta
160   algorithm was run with a maximum of 500 iterations and a p-value of 0.05. Only important features
161   were retained for further analysis. A further feature selection step removed correlated features from
162   the set of predictors used in the final model. Out of any two features with a correlation coefficient
163   above 0.7, only the feature with the higher importance measured as the mean decrease in accuracy
164   (see below) was retained in the final set of predictors. The variance inflation factor (VIF) was used as
165   an indicator to assess the remaining degree of multicollinearity in the data.

166   *2.8. Model fitting*

167   The random forest (RF) prediction algorithm [31] was chosen as the modelling tool for the
168   analysis because it has shown high predictive performance in a number of domains [32–35]. RF can
169   be used without extensive parameter tuning, it can handle a large number of predictor variables, is
170   insensitive to the inclusion of some noisy/irrelevant features,   makes no assumptions regarding the
171   shape of distributions of the response or predictor variables [36] and is therefore suitable for this
172   analysis. The RF is an ensemble technique that 'grows' many classification trees. Two elements of
173   randomness are introduced: Firstly, each tree is constructed from a bootstrapped sample of the
174   training data. Secondly, only a random subset of the predictor features is used at each split in the

175   tree building process. This has the effect of making every tree in the forest unique. The underlying
176   principle of the technique is that although each tree in the forest may individually be a poor
177   predictor and that any two trees could give different answers, by aggregating the predictions over a
178   large number of uncorrelated trees, prediction variance is reduced and accuracy improved [37: p.
179   316]. For binary classifications, probability predictions are initially derived based on the fraction of
180   votes given for a specified class by the ensemble of trees. These are subsequently dichotomised by
181   applying suitable thresholds (see below).
182       Two parameters can be specified when fitting a RF model. These are the number of trees to
183   grow ($n_{tree}$) and the number of features available for splitting ($m_{try}$). We varied $n_{tree}$ between 500 and
184   5000 (steps of 500) to investigate the effect on the accuracy and stability of the model. Varying $n_{tree}$
185   had little influence on model accuracy but model stability increased with the number of trees. We
186   selected $n_{tree}$ = 2000 as a compromise between stability and processing time. For $m_{try}$ the default
187   value, equal to the square root of the number of predictor variables (rounded down), was chosen.
188       RF also provides a relative estimate of predictor variable importance. This is measured as the
189   mean decrease in accuracy associated with each variable when it is assigned random but realistic
190   values and the rest of the variables are left unchanged. The worse a model performs when a
191   predictor is randomised, the more important that predictor is in predicting the response variable.
192   The mean decrease in accuracy was left unscaled, i.e. it was not divided by the standard deviation of
193   the differences in prediction errors, and is reported as a fraction ranging from 0 to 1.
194       The randomForest package [38], executed via the Marine Geospatial Ecology Tools v08a.67 [39],
195   was used for the implementation of the model.

*2.9. Spatial prediction*

197       The selected RF model was applied to the whole dataset to predict the probability of carbonate
198   mound presence for each image object. For the dichotomisation of the probabilistic outputs, a
199   threshold was calculated from the training data by maximising the Youden index [40].

*2.10. Model performance*

201       Model performance of presence-absence predictions was assessed with the receiver-operating
202   characteristic (ROC) curve by plotting sensitivity against 1 - specificity for various thresholds.
203   Sensitivity is the amount of true presence predictions as a proportion of the total number of presence
204   observations (Table 4 and equation 2). Specificity is the amount of true absence predictions as a
205   proportion of the total number of absence observations (Table 4 and equation 3). The area under the
206   ROC curve, or AUC, was used to assess the model performance. An AUC value of 0.5 is indicating
207   discrimination ability no better than random and a value of 1 is indicative of perfect discrimination.
208       We assessed the accuracy of the dichotomised predictions with three widely applied metrics,
209   which can be derived from a contingency table (Table 4), namely the overall accuracy (percent
210   classified correctly, PCC), sensitivity and specificity. PCC is the proportion of correctly classified
211   presences and absences. The accuracy metrics were calculated with the caret package [41] in R.

212   Table 4. Contingency table for presence-absence predictions and selected associated accuracy
213       metrics.

|  | **Observed absence** | **Observed presence** |
|---|---|---|
| **Predicted absence** | True negative (TN) | False negative (FN) |
| **Predicted presence** | False positive (FP) | True positive (TP) |

214

$$PCC = \frac{(TN + TP)}{(TN + FN + FP + TP)} \tag{1}$$

$$Sens = \frac{TP}{(FN + TP)} \tag{2}$$

217
$$Spec = \frac{TN}{(TN + FP)} \tag{3}$$

218

### 2.11. Confidence

220     The predicted probabilities were also employed to assign a confidence score to the outputs
221 similar to ref. [42]: To indicate high confidence in the absence of carbonate mounds, a sensitivity
222 value of 0.95 was selected. In other words, we requested that 95% of the predicted presence of
223 mounds is correct based on the test set. Likewise, to indicate high confidence in the presence of
224 mounds, a specificity value of 0.95 was required, equal to 95% of absence of mounds correctly
225 classified based on the test set. The choices for the selected values of sensitivity and specificity are
226 somewhat arbitrary here. However, they were selected for illustrative purposes and will be
227 discussed in greater detail later on. Additionally, we considered whether the predictions were
228 within or outside the modelled range of values of the RF model. Scores of 0 and 1 were given for low
229 and high confidence for both aspects of the predictive model and summed to give total confidence
230 scores of 0 (low confidence), 1 (medium confidence) or 2 (high confidence). The PresenceAbsence
231 [43] and ROCR [44] packages were used in R to calculate thresholds for required values of sensitivity
232 and specificity and create diagnostic plots.

### 2.12. Representation on maps

234     Since carbonate mounds are small features compared to the size of the study area, we represent
235 them in an aggregated form by calculating the fraction of mound area per 1 km$^2$ block. We also
236 display the mean total confidence score in a similar way.

### 3. Results

### 3.1. Feature selection

239     The Boruta feature selection reduced the number of predictor features from 24 to 22 (Figure 3).
240 Two features were deemed unimportant (Asymmetry, Main_direc). The subsequent correlation
241 analysis reduced the number of predictor features to six. All VIFs were below 3 indicating a low
242 degree of multicollinearity in the remaining predictors (Table 5). Mean_curPL, Mean_rgh,
243 Mean_curPR, Area_pxl, LengthWidt and Mean_bpi25 were used to build the final model.

244
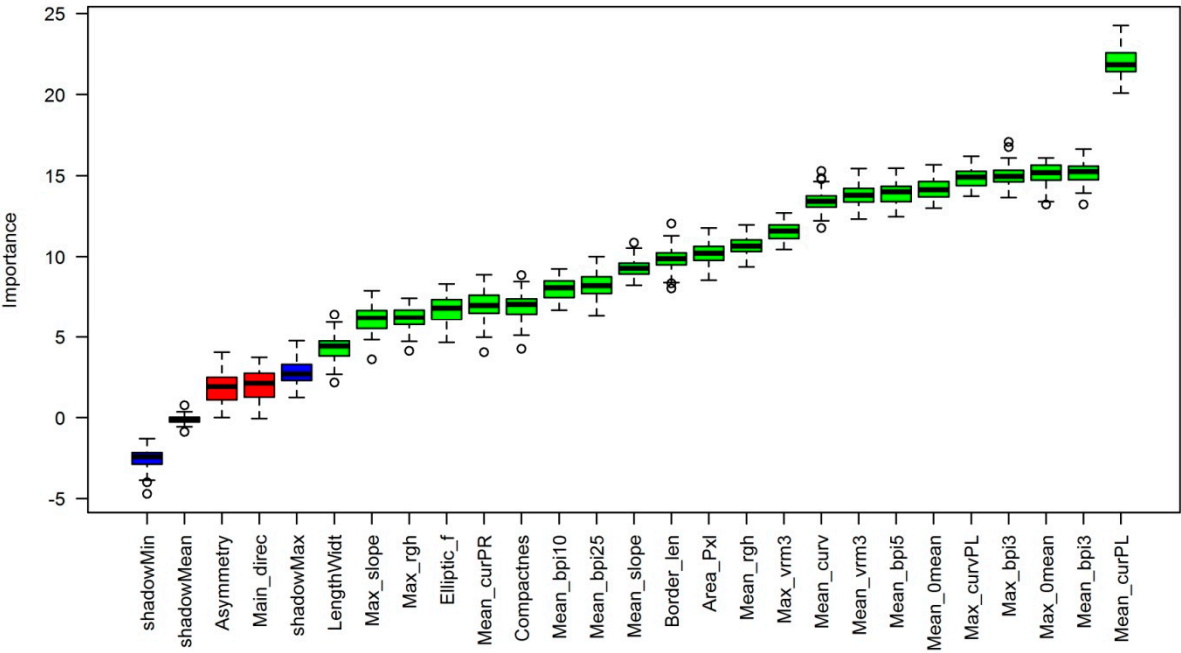
245     Figure 3. Results of the Boruta feature selection analysis. Green colours indicate important features,
246     red colours indicate unimportant features. Shadow features are shown in blue.

247     Table 5. Variance inflation factors for the selected features

| Feature | VIF |
|---|---|
| Mean_curPL | 2.654873 |
| Mean_rgh | 1.9249 |
| Mean_curPR | 2.250794 |
| LengthWidt | 1.133754 |
| Area_Pxl | 1.340249 |
| Mean_bpi25 | 2.28189 |

248     *3.2. Model performance and confidence*

249     The model had an AUC = 0.91, which indicates a well-performing model with excellent
250     discriminatory ability (Figure 4, top left). The probability threshold for maximising the Youden
251     index was 0.619. The selected threshold also coincided with a maximum in PCC (Figure 4, top right).
252     Probabilities above this threshold were classified as presence of carbonate mounds. Accuracy
253     statistics associated with this threshold are as follows: 84.4% of objects were correctly classified (PCC
254     = 0.844; 95% confidence intervals: (0.8003, 0.8811)). This is significantly higher (p < 2e-16) than the no
255     information rate (NIR = 0.574), which was taken to be the largest class percentage in the data. The
256     model had a high sensitivity (Sens = 0.827) and specificity (Spec = 0.866).

257
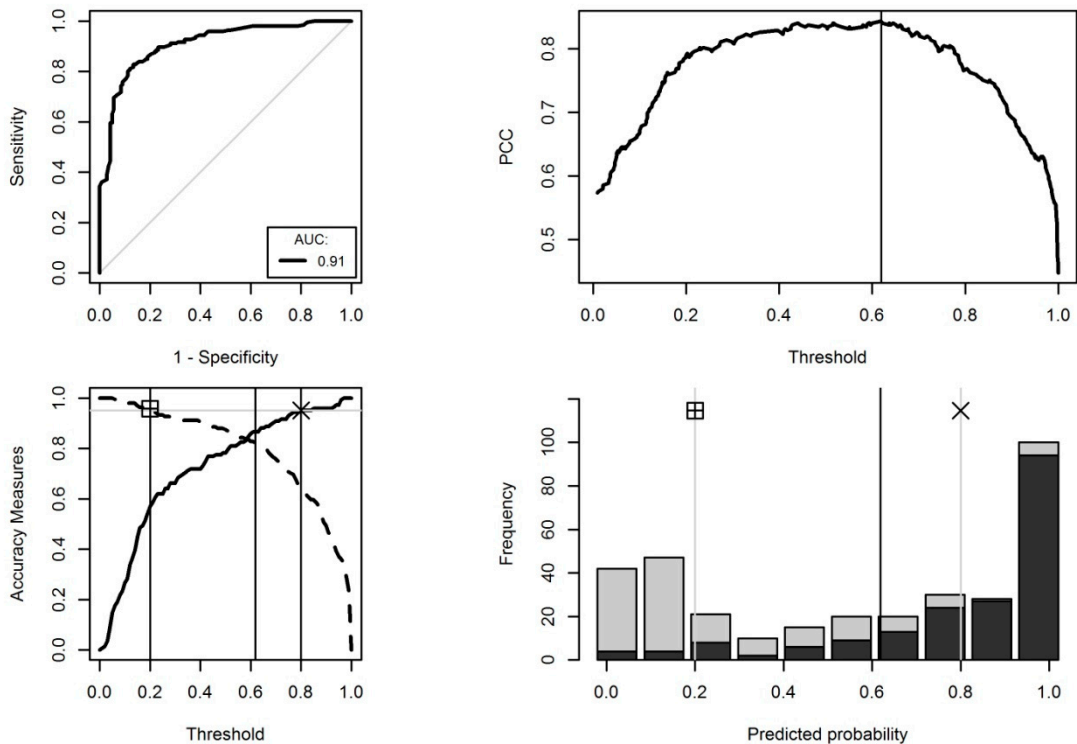
258     Figure 4. Summary of model performance: Top left – ROC curve (bold black line) indicating AUC =
259     0.91. The grey diagonal indicates AUC = 0.5 (no discrimination ability). Top right – PCC versus
260     selected threshold: The threshold selected by maximising the Youden index (0.619) gave the highest
261     PCC. Bottom left – Sensitivity (dashed line) and specificity (solid line) versus selected threshold:
262     Requesting Sens = 0.95 and Spec = 0.95 gave thresholds of 0.2 and 0.8, respectively. Bottom right –
263     Histogram showing the frequency of presence (black) and absence (grey) observations against the
264     predicted probability.

265        Probability thresholds for Sens = 0.95 and Spec = 0.95 were 0.20 and 0.80, respectively (Figure 4,
266    bottom left). These were employed to typify confidence in the predictions: Confidence is high for
267    probabilities below 0.20 (high confidence in absence) and equal to or greater than 0.80 (high
268    confidence in presence) as indicated by the low proportion of incorrectly classified objects seen in
269    Figure 4 (bottom right). Confidence is low for intermediate probability values. In 1.5% of the cases
270    were the predictions outside the range of modelled values, leading to low confidence in this aspect
271    of the model. Predictions were inside the modelled range for 98.5% of the cases and high confidence
272    was associated with these predictions. Total confidence was high in 67.42%, medium in 32.13% and
273    low in 0.45% of the cases.

274    *3.3. Spatial representation*

275        Figure 5 shows an example detail of the results with predicted carbonate mounds mapped with
276    three levels of total confidence. These are overlaid on a hillshade image of the bathymetry.

277
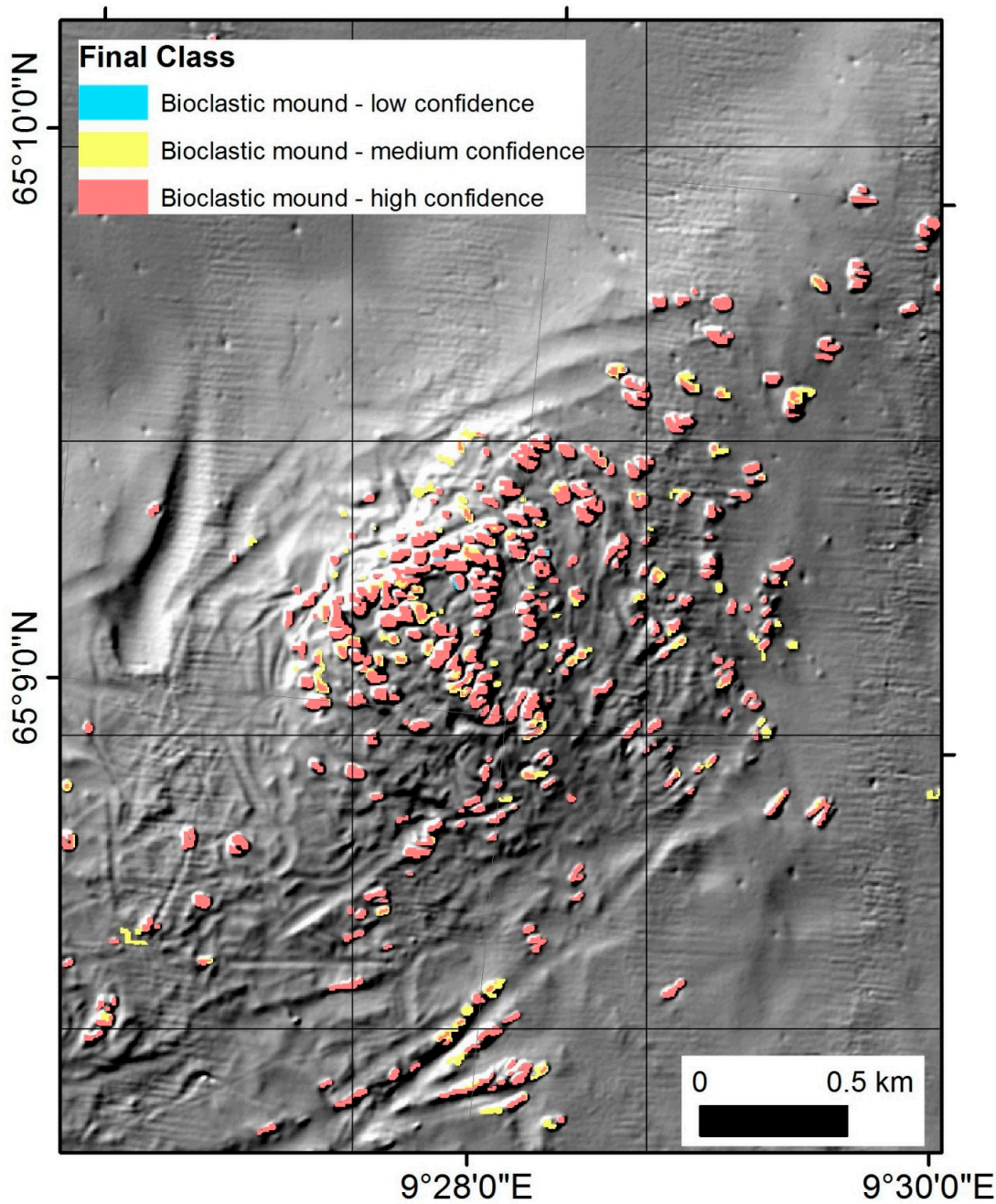
278    Figure 5. Left - Example detail of mapping results showing predicted occurrence of carbonate
279    mounds and associated total confidence overlaid on a hillshade image of the bathymetry. Also
280    visible is the 1 km by 1 km raster used to aggregate data on carbonate mounds.

281    The relative mound area (Figure 6) varies between 0% and close to 18%; however, the
282    distribution is uneven with mound areas below 1% in more than half of the blocks (and not
283    including blocks with a mound area equal to 0%). Mounds occur predominantly in a NNW-SSE
284    trending zone. Confidence in the predictions is high overall.

285
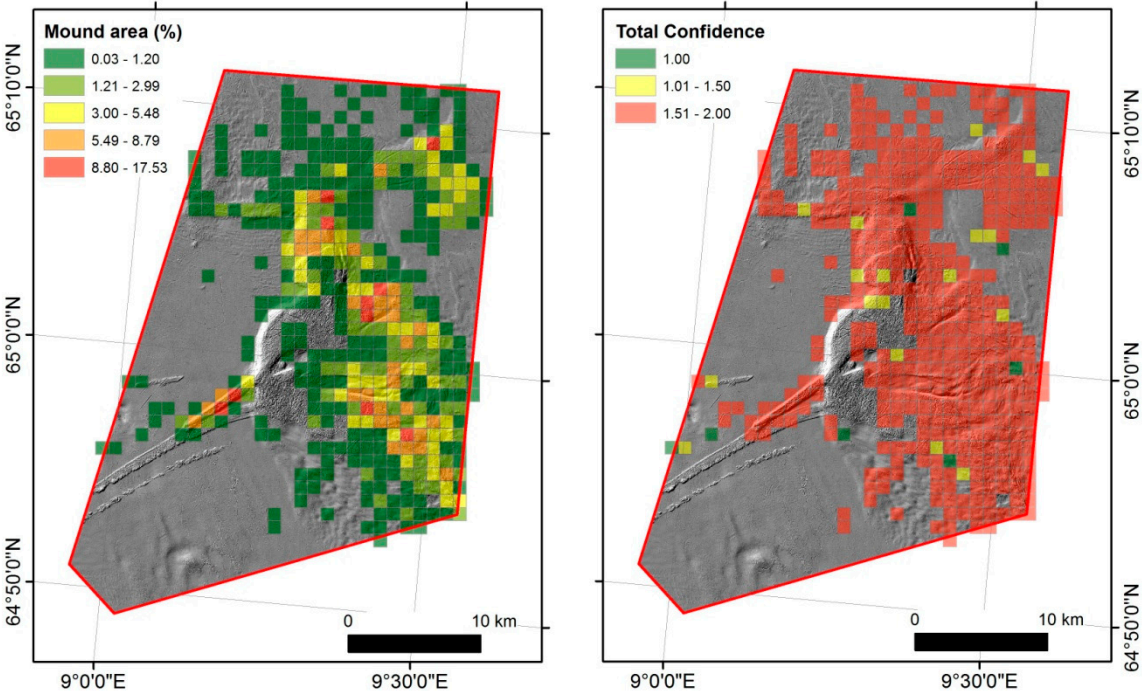
286    Figure 6. Left - Carbonate mound area per 1 km² block expressed as percentage of mound area per
287    block. Right – Average total confidence per 1 km² block. Only blocks that were occupied by at least
288    one carbonate mound are shown.

289    *3.4. Predictor feature importance*

290    Mean_curvPL was by far the most important predictor feature with a mean decrease in
291    accuracy of approximately 15% (Figure 7). Other features were significantly less important with
292    mean decreases in accuracy below 5%. However, it should be noted that other features that have
293    been removed from the model due to high correlation with those features included in the model may
294    also be useful predictors for carbonate mounds. Based on the feature importance scores of the Boruta
295    analysis (Figure 3), the most likely candidates are Mean_bpi3, Max_0mean, Max_bpi3, Max_curvPL,
296    Mean_0mean, Mean_bpi5, Mean_vrm3 and Mean_curv.

297    **4. Discussion**

298    We have demonstrated how carbonate mounds can be mapped from derivatives of MBES
299    bathymetry in an efficient and validated way with high accuracy by combining image segmentation
300    with presence-absence spatial predictions. This approach is reasonably quick; the most
301    time-consuming steps being data preparation (calculation of derivatives etc.) and classification of
302    sample objects, both of which took approximately one working day. All in all, it took about one
303    working week to derive the showcased maps. This is considerably faster than manual interpretation
304    of the MBES data.

305    Image segmentation was a vital step in the mapping approach for two reasons: First, it allowed
306    selecting sample objects for visual classification. Such a step would have been difficult to exercise
307    based on image pixels. Second, additional features other than image layer values were extracted and
308    utilised in the spatial prediction. The final model did not only include object mean values, but also
309    extent features, which contributed to the final predictions.

310
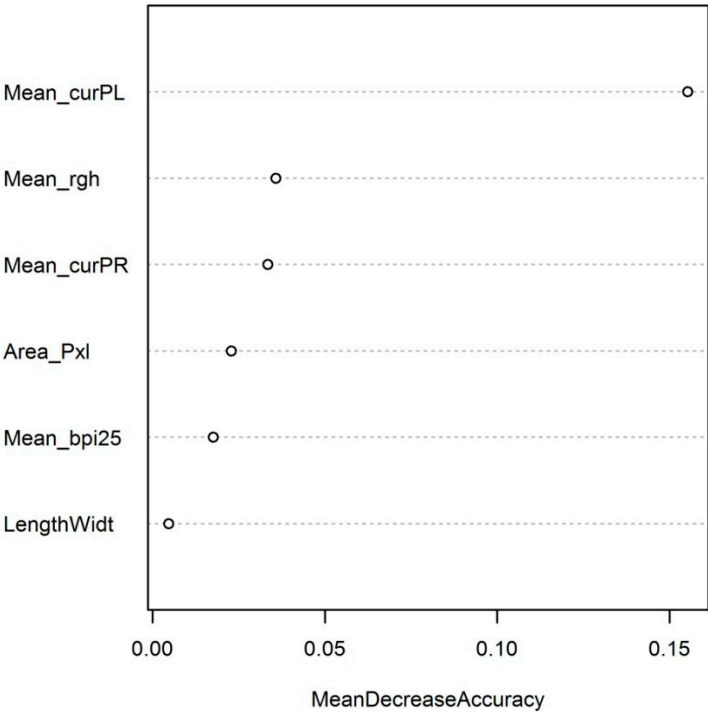
311    Figure 7. Predictor feature importance expressed as the mean decrease in accuracy when a feature is
312    randomised. Larger decreases mean that the feature is more important. The mean decrease in
313    accuracy ranges from 0 to 1.

314    We used a pre-existing bioclastic sediments [18] map layer as a spatial constraint for the
315    analysis. Although this might carry the risk of missing some of the mounds present in the area, we
316    judge the chances of this being the case as low. The main benefit of spatially constraining the
317    analysis were that the total number of image objects used in the analysis was markedly smaller
318    (23602 instead of 83085 image objects) and, more importantly, the presence-absence ratio was higher.
319    Initial trials without a spatial constraint at a different but similar site showed that it was still possible
320    to derive meaningful results with high accuracy, but more sample objects are required to give a
321    sufficiently high number of mound presences.
322    The predictive model was trained and tested with samples that were derived by visually
323    assessing a sub-set of image objects. This approach is arguably prone to introducing error due to the
324    incorrect classification of an unknown number of sample objects. However, we caution that
325    ground-truth information derived from underwater stills or video is equally not free of error due to
326    mis-classification [45]. Moreover, ground-truth information is often difficult and costly to obtain,
327    and these factors typically limit the number of samples available for an analysis. Our approach
328    allowed us to select a large amount of sample objects without the additional costs. We believe that
329    the approach was justified as carbonate mounds are typically conspicuous objects on the seabed
330    readily identifiable from MBES data but do not recommend utilising this approach in situations
331    where the target classes are less obvious.
332    It is important to assess the performance of a model to understand how reliable the predictions
333    are. In this case, discriminatory ability (AUC) and accuracy (PCC, Sens and Spec) of the predictions
334    were generally high. However, model performance statistics are either global or class-specific,

335    giving no information on the accuracy of the prediction in a spatially explicit way [46]. Maps that
336    portray the spatial variation of mapping error or uncertainty can be highly informative: They might
337    be used to guide future ground-truth sampling campaigns or provide managers with information on
338    the reliability of predictions when making decisions. Here, we have adopted and modified a scheme
339    to assess the confidence in spatial predictions developed for mapping bedrock outcrops on the
340    United Kingdom's continental shelf [42]. The confidence in the presence of carbonate mounds is
341    high where probabilities are 0.8 or higher and the predictions are within the modelled range of
342    values of the RF model. Medium confidence in the presence of carbonate mounds means that one of
343    the two criteria is not fulfilled, and low confidence is assigned when both criteria are not fulfilled,
344    but probabilities are higher than 0.619. In this way, we express confidence in the predictions in a way
345    that is simple to understand; yet, confidence is based on objective and measurable criteria rather
346    than scoring systems and it is spatially explicit.

347    As mentioned earlier, the choice of sensitivity and specificity values of 0.95 was somewhat
348    arbitrary and used for illustrative purposes. Preferably, the selection of those values should be
349    informed by the objectives of the mapping task. Increasing the value for the required specificity will
350    reduce the number of false positives, i.e. the number of image objects incorrectly classified as
351    carbonate mounds will be reduced. For example, increasing the required specificity from 0.95 to 0.99
352    will increase the probability threshold from 0.8 to 0.96. Consequently, the number of image objects
353    classified accordingly will be reduced from 10107 to 5868. This might be useful when a high level of
354    certainty in the presence of carbonate mounds is required, for example when a field survey is
355    planned, and targeted stations should correspond to carbonate mounds as frequently as possible.

356    This approach allows mapping carbonate mounds from MBES data with high accuracy and
357    confidence. Carbonate mounds are the geological product of CWCs [17]; however, it is important to
358    note that the cover of such mounds with live corals can vary dramatically. In fact, mounds might
359    exhibit live coral cover approaching 100% or be completely devoid of live corals, even in close
360    proximity, as shown by detailed results from the Mingulay Reef Complex west of Scotland [47].
361    Although it has been demonstrated that the likelihood of live coral presence can be spatially
362    predicted [47], it will still require detailed ground-truthing, for example with video or stills images,
363    to establish whether or not carbonate mounds are occupied by live corals and to what degree.

364    In this case study, Mean_curPL was by far the most important predictor for the presence of
365    carbonate mounds. However, other features relating to terrain variability, curvature and relative
366    position are expected to be suitable predictors for carbonate mounds as well, but were strongly
367    correlated with Mean_curPL and hence removed from the analysis.  The comparatively small size
368    of the mounds in relation to the resolution of the terrain data means that small neighbourhood sizes
369    of 3 and 5 were the most relevant. We recommend that other studies attempting to predict carbonate
370    mounds should consider features of terrain variability, curvature and relative position [22] at a
371    relevant scale that reflects both the size of the mounds to be mapped and the resolution of the data
372    utilised.

373    Future work will include a comparison of the results presented here with ground-truth
374    information from underwater video tows. This information might also be used to add another layer
375    of confidence: Image objects that coincide with interpreted video frames and agree with the
376    interpretation might be given a higher confidence score [42,48]. In a next step, the developed
377    methodology will be applied to areas of the Norwegian continental shelf and slope where MBES
378    data have been collected. Previous research has shown that carbonate mounds are identifiable from
379    MBES data in areas of flat seabed, iceberg ploughmarks and glacial lineations, while slide scar
380    environments and bedrock outcrops limit the ability to detect carbonate mounds [18]. To what
381    extent the presented method is capable of mapping carbonate mounds in such challenging
382    environments remains to be tested. Further work might include the extraction of additional
383    morphometric variables such as the maximum height of a mound above the surrounding seabed and
384    the volume of a mound. Such metrics could be used to derive the amount of inorganic carbon stored
385    in carbonate mounds on the Norwegian seabed, information that is critical for a better

understanding of the importance of CWC reefs as carbonate sinks [49] and possible impacts of climate change (warming and acidification) on those carbon stores [12].

**Supplementary Materials:** The following are available online at www.mdpi.com/link: RuleSetDocu.txt: Documentation of the eCognition rule-set (Chapters 2.3 – 2.5); Iverryggen_training_data.txt: Model training data set containing observed classes (carbonate mound presence and absence) and predictor feature values; FeatureSelection.r: R script for feature selection (Chapter 2.7); rf2000_2.Rdata: Output from MGET random forest model fitting (Chapter 2.8); rf2000_2_model_stats.txt: Model performance summary and confusion matrix  as provided by MGET; MapAccuracy.r: R script for calculation of accuracy statistics; rf2000_2_export_for_PresenceAbsence.txt: Text file containing observed classes (test data) and predicted probabilities; BinaryClassification.r: R script to derive thresholds for selected sensitivity and specificity and model performance plots (Chapter 2.10).

**Acknowledgments:** This study was funded by the Geological Survey of Norway. The bathymetry data were made available by the Norwegian Mapping Authority, Division Hydrographic Service, funded by the MAREANO programme.

**Author Contributions:** M.D. and T.T. conceived and designed the study; M.D. performed the analysis; M.D. analysed the data; M.D and T.T. wrote the paper.

**Conflicts of Interest:** The authors declare no conflict of interest. The founding sponsors had no role in the design of the study; in the collection, analyses, or interpretation of data; in the writing of the manuscript, and in the decision to publish the results.

# References

1.  Roberts, J. M.; Wheeler, A. J.; Freiwald, A. Reefs of the Deep: The Biology and Geology of Cold-Water Coral Ecosystems. *Science (80-. ).* 2006, *312*, 543 LP-547.

2.  Baillon, S.; Hamel, J.-F.; Wareham, V. E.; Mercier, A. Deep cold-water corals as nurseries for fish larvae. *Front. Ecol. Environ.* 2012, *10*, 351–356, doi:10.1890/120022.

3.  Costello, M. J.; McCrea, M.; Freiwald, A.; Lundälv, T.; Jonsson, L.; Bett, B. J.; van Weering, T. C. E.; de Haas, H.; Roberts, J. M.; Allen, D. Role of cold-water Lophelia pertusa coral reefs as fish habitat in the NE Atlantic. In *Cold-Water Corals and Ecosystems*; Freiwald, A., Roberts, J. M., Eds.; Springer Berlin Heidelberg: Berlin, Heidelberg, 2005; pp. 771–805 ISBN 978-3-540-27673-9.

4.  Auster, P. J. Are deep-water corals important habitats for fishes? In *Cold-Water Corals and Ecosystems*; Freiwald, A., Roberts, J. M., Eds.; Springer Berlin Heidelberg: Berlin, Heidelberg, 2005; pp. 747–760 ISBN 978-3-540-27673-9.

5.  Althaus, F.; Williams, A.; Schlacher, T.; Kloser, R. J.; Green, M.; Barker, B.; Bax, N.; Brodie, P. Impacts of bottom trawling on deep-coral ecosystems of seamounts are long-lasting. *Mar. Ecol. Prog. Ser.* 2009, *397*, 279–294.

6.  Hall–Spencer, J.; Allain, V.; Fosså, J. H. Trawling damage to Northeast Atlantic ancient coral reefs. *Proc. R. Soc. London. Ser. B Biol. Sci.* 2002, *269*, 507 LP-511.

7.  Fosså, J. H.; Mortensen, P. B.; Furevik, D. M. The deep-water coral Lophelia pertusa in Norwegian waters: distribution and fishery impacts. *Hydrobiologia* 2002, *471*, 1–12, doi:10.1023/A:1016504430684.

8.  Huvenne, V. A. I.; Bett, B. J.; Masson, D. G.; Bas, T. P. Le; Wheeler, A. J. Effectiveness of a deep-sea cold-water coral Marine Protected Area, following eight years of fisheries closure. *Biol. Conserv.* 2016, *200*, 60–69, doi:https://doi.org/10.1016/j.biocon.2016.05.030.

9.  Fisher, C. R.; Hsing, P.-Y.; Kaiser, C. L.; Yoerger, D. R.; Roberts, H. H.; Shedd, W. W.; Cordes, E. E.; Shank, T. M.; Berlet, S. P.; Saunders, M. G.; Larcom, E. A.; Brooks, J. M. Footprint of Deepwater Horizon blowout impact to deep-water coral communities. *Proc. Natl. Acad. Sci.* 2014, *111*, 11744–11749, doi:10.1073/pnas.1403492111.

10. Purser, A.; Thomsen, L. Monitoring strategies for drill cutting discharge in the vicinity of cold-water coral ecosystems. *Mar. Pollut. Bull.* 2012, *64*, 2309–2316, doi:https://doi.org/10.1016/j.marpolbul.2012.08.003.

11. Guinotte, J. M.; Orr, J.; Cairns, S.; Freiwald, A.; Morgan, L.; George, R. Will human-induced changes in seawater chemistry alter the distribution of deep-sea scleractinian corals? *Front. Ecol. Environ.* 2006, *4*, 141–146, doi:10.1890/1540-9295(2006)004[0141:WHCISC]2.0.CO;2.

12. Hoegh-Guldberg, O.; Poloczanska, E. S.; Skirving, W.; Dove, S. Coral Reef Ecosystems under Climate Change and Ocean Acidification. *Front. Mar. Sci.* 2017, *4*, 158.

13. Maier, C.; Watremez, P.; Taviani, M.; Weinbauer, M. G.; Gattuso, J. P. Calcification rates and the effect of ocean acidification on Mediterranean cold-water corals. *Proc. R. Soc. B Biol. Sci.* 2012, *279*, 1716–1723, doi:10.1098/rspb.2011.1763.

14. Büscher, J. V; Form, A. U; Riebesell, U. Interactive Effects of Ocean Acidification and Warming on Growth, Fitness and Survival of the Cold-Water Coral Lophelia pertusa under Different Food Availabilities. *Front. Mar. Sci.* 2017, *4*, 101, doi:10.3389/fmars.2017.00101.

15. Davies, A. J.; Wisshak, M.; Orr, J. C.; Murray Roberts, J. Predicting suitable habitat for the cold-water coral Lophelia pertusa (Scleractinia). *Deep Sea Res. Part I Oceanogr. Res. Pap.* 2008, *55*, 1048–1062, doi:10.1016/j.dsr.2008.04.010.

16. Davies, A. J.; Guinotte, J. M. Global Habitat Suitability for Framework-Forming Cold-Water Corals. *PLoS One* 2011, *6*, e18483.

17. Wheeler, A. J.; Beyer, A.; Freiwald, A.; de Haas, H.; Huvenne, V. A. I.; Kozachenko, M.; Olu-Le Roy, K.; Opderbecke, J. Morphology and environment of cold-water coral carbonate mounds on the NW European margin. *Int. J. Earth Sci.* 2007, *96*, 37–56, doi:10.1007/s00531-006-0130-6.

18. Bellec, V. K.; Thorsnes, T.; Bøe, R. *Mapping of bioclastic sediments - data, methods and confidence*; Trondheim, 2014;

19. Thorsnes, T.; Bellec, V.; Baeten, N.; Plassen, L.; Bjarnadóttir, L.; Ottesen, D.; Dolan, M.; Elvenes, S.; Rise, L.; Longva, O.; Bøe, R.; Lepland, A. The Seabed- Marine Landscapes, Geology and Processes. In *The Norwegian Sea Floor. New knowledge from MAREANO for ecosystem-based management*; Buhl-Mortensen, L., Hodnesdal, H., Thorsnes, T., Eds.; MAREANO, 2015; pp. 93–107.

20. Bjarnadóttir, L. R.; Ottesen, D.; Bellec, V.; Lepland, A.; Elvenes, S.; Dolan, M.; Bøe, R.; Rise, L.; Thorsnes, T.; Selboskar, O. H. *Geologisk havbunnskart, Kart 65000900, Mai 2017. M 1: 100 000*; 2017;

21. Buhl-Mortensen, P.; Buhl-Mortensen, L.; Dolan, M. Bottom Habitats and Fauna. In *The Norwegian Sea Floor. New knowledge from MAREANO for ecosystem-based management*; Buhl-Mortensen, L., Hodnesdal, H., Thorsnes, T., Eds.; MAREANO, 2015; pp. 108–115.

22. Wilson, M. F. J.; O'Connell, B.; Brown, C.; Guinan, J. C.; Grehan, A. J. Multiscale Terrain Analysis of Multibeam Bathymetry Data for Habitat Mapping on the Continental Slope. *Mar. Geod.* 2007, *30*, 3–35.

23. Sappington, J. M.; Longshore, K. M.; Thompson, D. B. Quantifying Landscape Ruggedness for Animal Habitat Analysis: A Case Study Using Bighorn Sheep in the Mojave Desert. *J. Wildl. Manage.* 2007, *71*, 1419–1426.

24. Lundblad, E. R.; Wright, D. J.; Miller, J.; Larkin, E. M.; Rinehart, R.; Naar, D. F.; Donahue, B. T.; Anderson, S. M.; Battista, T. A Benthic Terrain Classification Scheme for American Samoa. *Mar. Geod.* 2006, *29*, 89–111.

25. Krämer, K.; Holler, P.; Herbst, G.; Bratek, A.; Ahmerkamp, S.; Neumann, A.; Bartholomä, A.; van Beusekom, J. E. E.; Holtappels, M.; Winter, C. Abrupt emergence of a large pockmark field in the German Bight, southeastern North Sea. *Sci. Rep.* 2017, *7*, 5150, doi:10.1038/s41598-017-05536-1.

26. Hay, G. J.; Castilla, G. Geographic Object-Based Image Analysis (GEOBIA): A new name for a new discipline. In *Object-Based Image Analysis: Spatial Concepts for Knowledge-Driven Remote Sensing Applications*; Blaschke, T., Lang, S., Hay, G. J., Eds.; Springer: Berlin, 2008; pp. 75–89.

27. Blaschke, T.; Hay, G. J.; Kelly, M.; Lang, S.; Hofmann, P.; Addink, E.; Queiroz Feitosa, R.; van der Meer, F.; van der Werff, H.; van Coillie, F.; Tiede, D. Geographic Object-Based Image Analysis - Towards a new paradigm. *ISPRS J. Photogramm. Remote Sens.* 2014, *87*, 180–191.

28. Schiewe, J. Segmentation of high-resolution remotely sensed data - concepts, applications and problems. *Symp. Geospatial Theory, Process. Appl.* 2002.

29. Kursa, M.; Rudnicki, W. Feature selection with the Boruta Package. *J. Stat. Softw.* 2010, *36*, 1–11.

30. Guyon, I.; Elisseeff, A. An Introduction to Variable and Feature Selection. *J. Mach. Learn. Res.* 2003, *3*, 1157–1182.

31. Breiman, L. Random Forests. *Mach. Learn.* 2001, *45*, 5–32.

32. Prasad, A. M.; Iverson, L. R.; Liaw, A. Newer classification and regression tree techniques: Bagging and random forests for ecological prediction. *Ecosystems* 2006, *9*, 181–199, doi:10.1007/s10021-005-0054-1.

33.  Huang, Z.; Siwabessy, J.; Nichol, S. L.; Brooke, B. P. Predictive mapping of seabed substrata using high-resolution multibeam sonar data: A case study from a shelf with complex geomorphology. *Mar. Geol.* 2014, *357*, 37–52.

34.  Diesing, M.; Kröger, S.; Parker, R.; Jenkins, C.; Mason, C.; Weston, K. Predicting the standing stock of organic carbon in surface sediments of the North–West European continental shelf. *Biogeochemistry* 2017, doi:10.1007/s10533-017-0310-4.

35.  Che Hasan, R.; Ierodiaconou, D.; Monk, J. Evaluation of Four Supervised Learning Methods for Benthic Habitat Mapping Using Backscatter from Multi-Beam Sonar. *Remote Sens.* 2012, *4*, 3427–3443.

36.  Cutler, D.; Edwards, T.; Beards, K.; Cutler, A.; Hess, K.; Gibson, J.; Lawler, J. Random Forests for classification in Ecology. *Ecology* 2007, *88*, 2783–2792.

37.  James, G.; Witten, D.; Hastie, T.; Tibshirani, R. *An Introduction to Statistical Learning*; Springer, 2013; ISBN 9781461471370.

38.  Liaw, A.; Wiener, M. Classification and regression by randomForest. *R News* 2002, *2*, 18–22, doi:10.1159/000323281.

39.  Roberts, J. J.; Best, B. D.; Dunn, D. C.; Treml, E. A.; Halpin, P. N. Marine Geospatial Ecology Tools: An integrated framework for ecological geoprocessing with ArcGIS, Python, R, MATLAB, and C++. *Environ. Model. Softw.* 2010, *25*, 1197–1207, doi:10.1016/j.envsoft.2010.03.029.

40.  Perkins, N. J.; Schisterman, E. F. The inconsistency of "optimal" cutpoints obtained using two criteria based on the receiver operating characteristic curve. *Am. J. Epidemiol.* 2006, *163*, 670–675, doi:10.1093/aje/kwj063.

41.  Kuhn, M. Building Predictive Models in R Using the caret Package. *J. Stat. Software; Vol 1, Issue 5* 2008.

42.  Downie, A. L.; Dove, D.; Westhead, R. K.; Diesing, M.; Green, S.; Cooper, R. Semi-automated mapping of rock in the North Sea. *JNCC Rep.* 2016, *592*, doi:10.13140/RG.2.2.15199.05286.

43.  Freeman, E. A.; Moisen, G. PresenceAbsence: An R Package for Presence Absence Analysis. *J. Stat. Software; Vol 1, Issue 11* 2008.

44.  Sing, T.; Sander, O.; Beerenwinkel, N.; Lengauer, T. ROCR: visualizing classifier performance in R. *Bioinformatics* 2005, *21*, 3940–3941, doi:10.1093/bioinformatics/bti623.

45.  Rattray, A. J.; Ierodiaconou, D.; Monk, J.; Laurenson, L.; Kennedy, P. Quantification of Spatial and Thematic Uncertainty in the Application of Underwater Video for Benthic Habitat Mapping. *Mar. Geod.* 2014, *37*, 315–336, doi:10.1080/01490419.2013.877105.

46.  Diesing, M.; Mitchell, P.; Stephens, D. Image-based seabed classification: what can we learn from terrestrial remote sensing? *ICES J. Mar. Sci.* 2016, *73*, 2425–2441, doi:10.1093/icesjms/fsw118.

47.  De Clippele, L. H.; Gafeira, J.; Robert, K.; Hennige, S.; Lavaleye, M. S.; Duineveld, G. C. A.; Huvenne, V. A. I.; Roberts, J. M. Using novel acoustic and visual mapping tools to predict the small-scale spatial distribution of live biogenic reef framework in cold-water coral habitats. *Coral Reefs* 2017, *36*, 255–268, doi:10.1007/s00338-016-1519-8.

48.  Lillis, H. A three-step confidence assessment framework for classified seabed maps. *JNCC Rep.* 2016, *591*.

49.  Titschack, J.; Baum, D.; De Pol-Holz, R.; López Correa, M.; Forster, N.; Flögel, S.; Hebbeln, D.; Freiwald, A. Aggradation and carbonate accumulation of Holocene Norwegian cold-water coral reefs. *Sedimentology* 2015, *62*, 1873–1898, doi:10.1111/sed.12206.